Correlative Analysis Among experimental and Theoretical Structural, Thermochemical, and Molecular Spectroscopic Parameters of Crystals of Mandelic Acid

Bojidarka Ivanova *

Posted Date: 7 January 2025

doi: 10.20944/preprints202501.0504.v1

Keywords: Mandelate crystals; experimental and theoretical electron density analysis; thermochemistry; optical spectroscopy; chemical crystallography; quantum chemistry

 doi:10.20944/preprints202501.0504.v1

Article

Correlative Analysis Among experimental and Theoretical Structural, Thermochemical, and Molecular Spectroscopic Parameters of Crystals of Mandelic Acid

Bojidarka Ivanova

Lehrstuhl für Analytische Chemie, Institut für Umweltforschung, Fakultät für Chemie und Chemische Biologie, Universität Dortmund, Otto-Hahn-Straße 6, 44221 Dortmund, Deutschland;
bojidarka.ivanova@yahoo.com or b_ivanova@web.de

Abstract: Crystals of mandelic acid are of significant importance. They are commercial pharmaceutics formulations modulating active ingredient solubility and its pharmacological effect. Commercial pharmaceuticals are at about 50 % crystals. Salt formulation is among the most used strategy for improving properties of medications. Salt crystallization screening is routinely implemented into pharmaceutical industry. Via disproportionation there is produced free therapeutics forms. The process is thermodynamically and kinetically driven. It is tackled by crystallographic and quantum chemical methods for salt screening as integral parts of development workflow in pharmaceutical industry. Correlations among crystallographic, Fourier-transform infrared, and electronic spectroscopic data on salts, and theoretical thermochemical approaches are of primary importance for determining relations among molecular structure ↔ crystal structure ↔ properties of crystals. This paper presents novel structural and molecular spectroscopic data on crystals of mandelic acid such as DL-mandelic acid (1), 4-phenyl-pyridinium mandelate mandelic acid (2) — first, reported, herein, — and catena-((μ3-DL-mandelato)-silver(I)) (3). It also utilizes chemometrics. The major conclusion follows from relation between crystallographic potential energy data on bond critical point using Abramov's formula and theoretical bond dissociation energy showing |r|=0.9999. The approach seems best characterizes experimental crystallographic energetics of chemical bonds of molecules fitted off theoretical data.

Keywords: Mandelate crystals; experimental and theoretical electron density analysis; thermochemistry; optical spectroscopy; chemical crystallography; quantum chemistry

1. Introduction

A great deal of ongoing pharmaceutical research documentation indicates that the programmes for molecular drugs-design and screening of novel pharmaceutical formulations consists of significant number of research and development stages including preclinical and clinical phases, crossing at about ten years. The commercial availability of novel medication also depends upon its so-called dosage form. It determines the therapeutics' effectiveness, its side effects, or toxicity. The elaboration of the dosage form depends upon many factors. The most important one appears the physicochemical properties of the medication in the pharmaceutical formulation. Currently, there are at about 90 % novel medications in the discovery pipelines of the pharmaceutical industry. However, at about 40 % of the marketed therapeutics suffer from low aqueous solubility [1–5]. Despite the fact that there are developed novel drug delivery approaches including lipid-based pharmaceutical formulations or injections the oral solid dosage form is regarded as most conventional and preferred

 doi:10.20944/preprints202501.0504.v1

from patients' delivery system. Furthermore, the latter form is cost-efficient in addition to the fact that it is easy to commercial manufacturing. Owing to the fact that the pharmaceutical industry highlights increasing in the global market of the dosage form of oral solids within 2017–2027 [6], the research effort is focuses on developing of solid dosage forms of the novel medications; thus, overcoming barrier of medication's solubility and its permeability issue. From both the research and development perspective of commercial pharmaceutical formulations there have been elaborated a set of research strategies used to improve the physicochemical properties of the medications in their solid-dosage forms. For instance, these are pH modification of the analytes (co)-crystalizing as salts; co-crystallization of analytes and neutral species in crystals of pharmaceutical formulations; solid dispersions of components; polymeric micelles; inclusion complexes of embedded medication into biologically active macromolecules; solid lipid nanoparticles; self-emulsifying drug delivery systems, particle size reduction and nanonization, micro emulsions, and more. Particularly, the concept of (co)crystallization of medications has been recognized by the European Medicines Agency. According to the regulatory classification of the commercial pharmaceutical formulations the co-crystals are defined as crystalline materials containing two or more different molecules one of which is the medication within the framework of a defined stoichiometric ratio, crystal lattice interacting mutually via nonionic and noncovalent interactions. The definition as it has been developed excludes from so-called polymorphs or crystalline materials of the same analytes showing different packing. The crystalline form of the commercial medications, therefore, is regarded as most suitable one for control of physico-chemical properties of the therapeutics and their delivery. Due to these reasons, significant amount of research efforts of crystal engineering are concentrated on elaborating of novel crystalline forms of therapeutics via modulating physico-chemical properties of medications and improving their solubility, stability, permeability, bioavailability, and more; thus, achieving their enhanced therapeutic efficacy [2–5]. Thus, innovations in the field of crystal engineering involve strategies to pharmaceutical formulations of medications via co-crystal or salt formation which are based on tuning of intermolecular interactions. The comprehensive understanding of the driving forces governing the intermolecular interactions of are essential in the context of drug design and development, because of as aforementioned the achievement of the desirable pharmacological properties of the active ingredient are imperative for the pharmaceutical industry and the clinical practice. The research practice involves both experimental and theoretical approaches where computed properties of crystals of salts are validated by comparison with experimental data [7,8].

From the perspective of the current study, there lies the question: To what extent there is needed an in-depth study of molecular structure and optical spectroscopic properties of crystals of mandelic acid (MA; (1)) (2-hydroxy-2-phenylacetic acid (1) (Figure 1)? As an effort to address briefly the latter question and the issue, because of a comprehensive discussion proportionating to its significant impact on different fields of research is incapable of reflecting all dimensions of its significance for fundamental science and technological-application aspects, the introductory section shall only sketch that MA is of significant importance, due to: (i) its already common used to pharmaceutics formulations [9,10]. It is a frequent choice, amongst others, as co-crystalizing agent or counter ion of salts of pharmaceutical formulations due to its low toxicity and cost as well as readily availability on an industrial scale [11–13]. It is utilized to methenamine commercial pharmaceutics, which exhibit antibacterial prodrug biological activity against Escherichia coli [14]. The acidic properties of (1) (pKa1=3.4 [5]) promote urine acidification and; thus, promoting methenamine hydrolysis. The (1) is involved in pharmaceutical formulations of aripiprazole [5], trimethoprim [15], or baclofen [16], as well. The former medication is a third-generation antipsychotic drug used in the treatment of schizophrenia, depression, and bipolar disorder [5] acting as acts as agonist of dopamine D_2 and D_1 receptor subtypes [5]. The trimethoprim exhibits antimicrobial biological activity and is synthetic agent inhibiting bacterial dihydrofolate reductase enzyme [15]. The latter analyte treats muscle spasticity [16]. The MS conformers have been implemented into formulations with meloxicam, nicotinamide, meloxicam, levetiracetam, or isoniazid, as well [15]. Mandelic acid-based spirothiazolidinones are target agents against *M. tuberculosis* [17]. The co-crystallization of the

 doi:10.20944/preprints202501.0504.v1

medications with MA is governed by the fact that one of the important factor in obtaining efficacious concentration of the active component; and, thus to produce desirable pharmacological effect is as aforementioned solubility [1,18]. Theoretical modeling of the crystal growth of MA has been detailed on [7,8].

Further: (ii) The chirality is regarded as a key issue of the biological systems, because of a large number of the biological processes are chirality dependent. The biochemical reactions in the living systems are highly enantio-selective. Inappropriate molecular chirality might induce severe abnormalities. Thus, pharmacological activity and the metabolism in addition to the toxicological effects of different enantiomers of medications might drastically differ in humans [19]. Even, there are cases when one enantiomer of therapeutics treats diseases, while its other enantiomer can induce toxic or adverse side pharmacological effect. In the case of MA, enzymes from bacteria; for instance, *Pseudomonas* species, *Lactobacillus curvatus*, *Alcaligenes bronchisepticus*, and more show stereo selective oxidation for MA and; thus, are used to chemical synthesis of S-MA and R-MA enantiomers [20]. The stereo selective metabolism of MA in kidney and liver of rats shows that S-MA can be metabolized to phenyl glyoxylic acid as its major metabolite [20]. Therefore, the chirality has important implications in the field of the pharmaceutical industry, as well [21–23]. The utilization of enantiopure components into the pharmaceutical formulations is the most reliable approach to guarantee effectiveness of medications. Despite the fact that enantiomers show identical physico-chemical properties they exhibit different biological activities. Thus, at about 56% of active pharmaceutics available on market have a chiral center [24]. At about 94% of the novel commercial drugs formulations having active ingredients containing chiral center are enantiopure [24]. Due to these reasons cost-effectively appears use of naturally occurring chiral molecules as components of pharmaceutical solids. The MA is the latter context is also promising chiral molecular template allowing design and synthesis of chiral co-crystals and coordination polymers with metal ions via multiple binding centers and capability of formation of chelate structures. There are, so far, designed coordination polymers of MA showing stereo selective guest uptake and implementation into chiral separation technologies [21–23,25]. The chelating capability of MA toward metal ions is used to reduce calcium ion concentrations in vivo, as well.

The MA is also (iii) important raw material utilized as attractive molecular template for drugs-design of novel medications. As terminal functional group it is attached to innovative class of medications derivatives of MA suppressing virulence of *Ralstonia solanacearum* [26,27]. The latter species is soil-borne bacterium causing for a disease called 'bacterial wilt' affecting at about 200 plant species, including commercial crops such as tomatoes, tobacco, and potatoes. A class of MA-derivatives are used to suppress virulence via T3SS against Citrus canker [28] which is a highly contagious bacterial disease due to *Xanthomonas citri* subsp. to citrus crops. The MA is also used as an important chiral intermediate in pharmaceutical industry for the synthesis of cephalosporins [20,29] and nafithromycin [30]. There are also designed a series of novel MA-based peptidomimetic derivatives inhibiting the aminopeptidase N, which is expressed in brain and epithelial cells of the kidney, among others [31].

As an α-hydroxy acid, the (1) has a variety of further applications to (iv) dermatology, mainly due to its antibacterial properties [20,32–34]. The MA shows antioxidant effect, as well [25]. Lately, it has gained increasing popularity as a skin care treating agent for adult acne [32].

The (v) enantio-separation of MA as α-hydroxy acids is essential process because of it enantiomers are used as disease biomarkers for clinical diagnostics and prognosis of many diseases such as cancer, kidney diseases, brain diseases, diabetes, and more [31]. The MA is routinely determined in the clinical practice as urinary metabolite to chronic kidney failure [35,36]. It is used as a biomarker of the exposure of styrene, which is classified as a class of hazardous environmental pollutants, as well [20,37,38]. It is determined routinely vinyl mandelic acid in thyroid cancer management, as well [39].

To look forward at application-oriented aspects of MA there should be emphasized (vi) its importance for innovations regarding environmental clean-up technologies. The replacement of

 doi:10.20944/preprints202501.0504.v1

traditional petrochemical-based plastics [40,41] has currently driven the enormous search for corresponding green substitutes or so-called eco-friendly bioplastics. Thus, poly(L-lactic acid) is considered as prospective biodegradable and biocompatible alternative as the starch-based bioplastics [40,41]. However, these prospective biopolymers show poor crystallization kinetics; thus, limiting their applications. An enhancement of the crystallization capability is achieved via nucleating agents such as transition metal complexes of α-hydroxy acids such as mandelic acid [42]. Despite, as natural [25] and eco-friendly organic acid MA shows high selectivity and efficiency in reaction of hydrolysis of hemicellulose; thus, making it a prospective candidate for xylooligosaccharides production, as well [43,44].

Further, crucial advantage of the MS is (vii) its capability of polymerizing; thus, producing poly(mandelic acid) which itself is an aryl analogue of poly(lactic acid) and also appears a biodegradable analogue of polystyrene. The synthetic scheme involves stabilization of MA adducts with pyridine-containing bases for mechanisms of ring-opening polymerization reaction of MA. Its impressive advances showing comparable physical and mechanical properties of poly(mandelic acid) with polystyrene [45,46], however, the developed, so far, synthetic schemes requires high-boiling solvents in addition to isolation of poorly soluble product in moderate yields.[47,48]. Despite, the poly(mandelic acid) is regarded as potential biodegradable plastics for hot-food packaging industry.

Particularly, the interest in (viii) self-assembling processes of crystals MS, pyridine containing counter ions, and transition metal ions have attracted further much attention for designing of novel topological networks of crystals [49]. Despite the fact that, interest in MA crystals with pyridinium containing ligands (ix) is governed by not only the capability of MA to form homopolymer, but also the capability of corresponding pyridinium counter ions to produce [2+2] photo dimerization products depending on the experimental conditions of crystal growth. The latter issue is evergreen topic one in crystal engineering of organics, due to their emergent photomechanical properties and a great scale of technological applications [50–52]. The key of the experimental crystallographic knowledge of ionic interactions of MA and 4-phenylpyridine is the fact that the latter analyte appears inhibitor of palmitoleoyl-protein carboxylesterase [53]. In addition, its is an exogenously compound which can be found, amongst others, in oranges [54]. Owing to the fact that it likely to across the blood brain barrier there is observed its methylation by nicotinamide N-methyl transferase. The accumulation of the latter analyte causes for toxicity.

Furthermore, the MA and its derivatives have also found place as modifiers for asymmetric catalytic hydrogenation of ketopantolactone, for instance [55] and for high performance NiOx-based perovskite solar cells [56].

The sketched above application oriented aspects of MA for many interdisciplinary research fields particularly highlighting the fields of pharmaceutical industry and medicine do not, in fact, tell us what are the real dimensions of its advantages and applications. For the latter purposes it should be more useful to the readers to review the available literature which is out of the scope of the current study.

However, the introductory section begins with the use of MA of many salt crystallization reactions of commercially available pharmaceutical formulations. The later issue pertains to the generation of theoretical and experimental knowledge of the relations among molecular and electronic structures↔crystal structue↔properties of MA-crystals which are most relevant to understand the governing forces and both the molecular and factors determining the intramolecular, respectively, intraionic interactions of crystals of the discussed analyte which are directly relevant to the field of crystal engineering of pharmaceutical formulations and development of novel crystalline forms of therapeutics via modulating physico-chemical properties of the molecular species. In connection with the later research tasks there are folded together the production of both the theoretical and experimental scientific knowledge with its justification of claims based on empirical validation of theoretical data based on quantitative criteria of chemometrics. At this point the introductory section goes to focus on experimental and theoretical approaches used to provide knowledge of the aforementioned relations; thus, highlighting the high resolution single crystal X-

 doi:10.20944/preprints202501.0504.v1

ray diffraction, Fourier-transform infrared and electronic absorption spectroscopies and methods of quantum chemistry among others, because of they are infrequently uncertain to produce reliable experimental scientific conclusion or claim regarding the discussed relationships. Despite the fact that the traditional viewpoint is that our knowledge based on these approaches is not fragile, but, rather it is regarded as stable one, this paper provides novel structural and spectroscopic experimental and theoretical data together with thermochemical ones on DL-mandelic acid (1), 4-phenyl-pyridinium mandelate mandelic acid (2), and AgI-complex of mandelic acid (3) discussing the absolute assurance connected with the matter of facts into the process of generation of the experimental scientific knowledge with is of paramount importance for the topic fields of pharmaceutical industry and medicine. The major purpose of the study fails to provide skeptical point of view regarding these robust methods for molecular structural analysis of crystals, but, rather to presents novel results from the continual, in fact, calibration of these experimental and theoretical tools; thus, discussing the uncertainty of knowledge of these approaches and generating conviction regarding what we know reliably as experimental data and what we do not know sure. The latter issue is best characterized by assessment of reliability of the experimental knowledge via application of different methods for processing of experimental data on crystals and various theoretical quantum chemical tools tackled by means of methods of chemoimetrics; thus, determining the reliability of the data or their scientific acceptability.

2. Results

2.1. Crystallographic Data

The polymorph I of DL-mandelic acid (1) crystalizes into orthorhombic space group type Pbca at ambient experimental conditions determined by single crystal X-ray and neutron diffraction studies [57–65] (Figures 1, S1 and S2; Table 1). There is also high pressure polymorph II showing monoclinic space group type $P2_1/c$ [58,63]. The intermolecular interactions of polymorph II cause for hydrogen-bonded double chains of MA-molecules along a-axis. Its crystal structure is markedly different from polymorph I showing a close relationship to crystallographic packing of MA-crystals of its pure enantiomers, rather than to it crystals of racemate [63]. The polymorphism as crystallographic phenomenon accounts for molecular capability to crystalize in more than one crystal structures depending on packing properties of molecules due to their intermolecular interactions [66–70]. The properties of corresponding polymorph modifications could vary broadly including their molar volume; crystal density; refractive index; packing properties; thermal and electric ones; hygroscopicity; conductivity; and more, all associated with thermodynamics; kinetics; surface and mechanical properties of crystals. Thus, the phenomenon becomes an important task to manufacturing pharmaceutics. The MA-polymorphism has been comprehensively studied [58,59,71] including upon its affect on temperature and pressure. As has been shown [58] there is polymorph transition between the latter two polymorphs at P=0.65 GPa and at T=460 K. Therefore, due to reasons sketched above this study lacks of description of intramolecular interactions of (1) in crystals.

 doi:10.20944/preprints202501.0504.v1

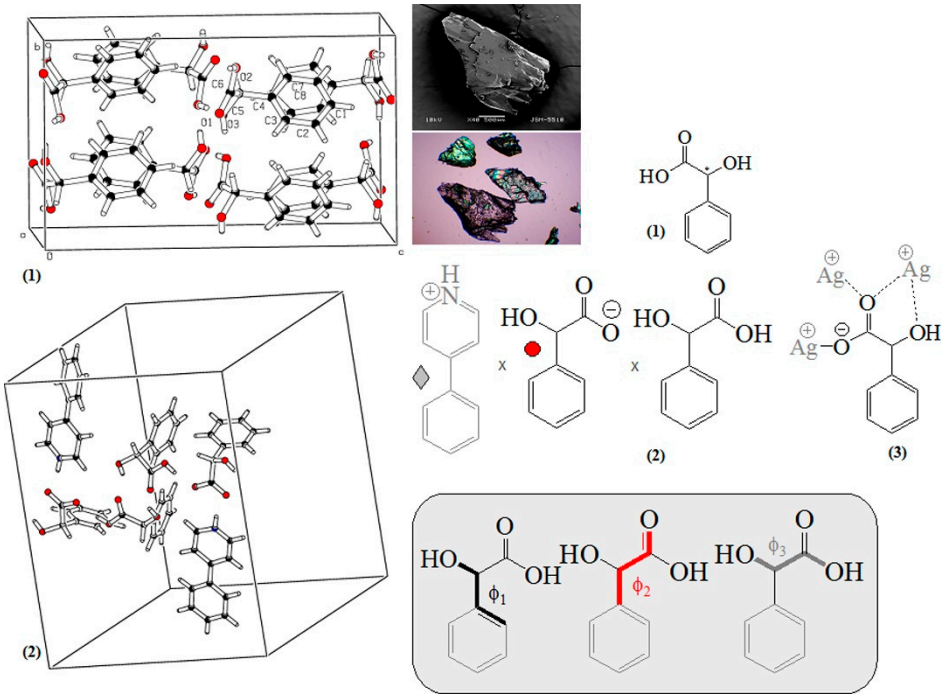

Figure 1. ORTEP plots of unit cell contents of crystals (1) (CCDC 880481) [57] and (2) (CCDC 822753) (this work); chemical diagrams of crystals (1)–(3); name definitions of dihedral angles of mandelic acid; photograph and scanning electron microscopic image of crystals.

Rather, it concentrates on novel data on complementary employment in experimental and theoretical electron density analyses and electrostatic surface potential (ESP) results aiming at further understanding of relation between molecular and electronic structures↔crystal structue↔properties of (1) because of it determines its diversity of (biological) activity including catalytic properties. The MS-derivatives exhibit a diversity of crystal structures and unusually complex packing in crystals; furthermore, showing small energy difference among polymorphs [72]. The latter property of MA and its analogous determined a significant structural both bulk and surface diversity, as well. The same is valid to refined, so far, crystal structures of disordered mandelic acids showing that energy differences between these disordered structures can vary with the framework of computational methods, as well. As can be expected, computations accounting for environmental effects such as solvent polarity, temperature, ionic strength, and more, which are of primary importance looking at application-oriented aspects of the study; thus, affecting on energetics of hydrogen bonded structural motifs of MA containing crystals. Looking at the major goal of the study one could further conclude that the focus underlines the relationship between molecular and crystal structure as well as spectroscopic properties.

In conjunction with purposes of the study, first, there should be considered functional relationships between experimental crystallographic and theoretical data on electronic structures or electron density distribution of atoms in molecules within the framework of 3D space of MA- crystals because of electronic interactions of crystals determine electronic absorption spectra and vibration characteristics of the molecules within the concept of chemical bond [73].

In addition, the electron density distribution is of fundamental importance for understanding the mechanisms of chemical reactions, respectively, biological activity of species, because of within the thermodynamic approach assessing energetics of electronic interactions of species via parameters enthalpy reflecting energetics of chemical bond and entropy accounting for environmental factors there is direct correlation between molecular structure↔(hydrogen) bonding interactions↔energetics with experimentally measured IC_{50} or the so-called transfer function [74–76].

 doi:10.20944/preprints202501.0504.v1

Thus, experimental crystallographic and theoretical electronic structural analysis of nature of inter-atomic, respectively, inter-molecular interactions in molecules and their crystals reveal the actual dimension of study ranging from determining of experimental electron density of atoms in the molecules to their biological function only assessing the aforementioned correlation quantitatively.

From both experimental and theoretical perspectives the study of electron density distribution via crystallography is based on the concept of electronic charge distribution around atoms in molecules [73].

Thus, the distribution of the total charge of all molecules in the unit cell of their crystal is determined using atomic positions within the 3D space, their thermal vibrations, and corresponding electronic charge parameters [77–80]. The models of these parameters are fitted off experimental crystallographic data by least squares. The obtained mapped electrostatic properties of crystals in 2D or 3D space (Figures S1 and 2) which can be obtained both experimentally via crystallographic methods; and, theoretically via computational quantum chemistry determined the line formed between theoretical and experimental electron density distribution of molecules in crystals. There is established the link between experimental and theoretical 3D conformational and electronic structure of molecules. From the perspective of chemical reactivity important parameters appears electrostatic potentials because of on the one hand they are derived from experimental crystallographic data. On the other hand they can be highly accurately determined via methods of computational quantum chemistry. The ESP maps (Figure 3), thus, illustrate regions of electronegativity and electro positivity of molecules. These regions are not easily inferred from analysis of parent charge density distribution. In the latter context, the ESP mapped on the so-called Hirshfeld surfaces provide direct link into intermolecular interacting ensembles of crystals [81–86]. The Hirshfeld surface is determined as an attempt to define the 3D space occupied by molecules; thus, partitioning the corresponding crystal electron density into the different molecular fragments of crystals. In parallel, there should be highlighted the Bader's quantum theory of atoms in molecules developed as an effort on determining the experimental electron density of atoms of the molecules. An important connecting emphasis at this point is that despite the fact that these theories provide crucial knowledge of the molecular structure of the crystals both experimentally and theoretically, thus, making them highly attractive for a practical explanation and prediction of intermolecular interactions in crystals, they direct application is far from trivial one. In the later context there is not supposed limits of the various theories but rather underlying that it might not be so intelligible to apply them directly, because of if there is concentrate on the Hirshfeld surfaces then the introduced weight function defined within the framework of the molecules of the crystals and determining the molecular properties by integration over the weighted electron density depends on the diffusion properties of the atoms in the molecules (see equation (2) in work [87]). From the point of view of methodology the latter statement is an attempt to underline the fact that accurate prediction of Hirshfeld atomic charges via quantum chemical methods should depend on the theoretical level. Turning to correlation between comparative analysis between theoretical and experimental crystallographic electron densities and charges it appears clear that the reliability of the theoretical data depends on the accuracy of the computational methods.

 doi:10.20944/preprints202501.0504.v1

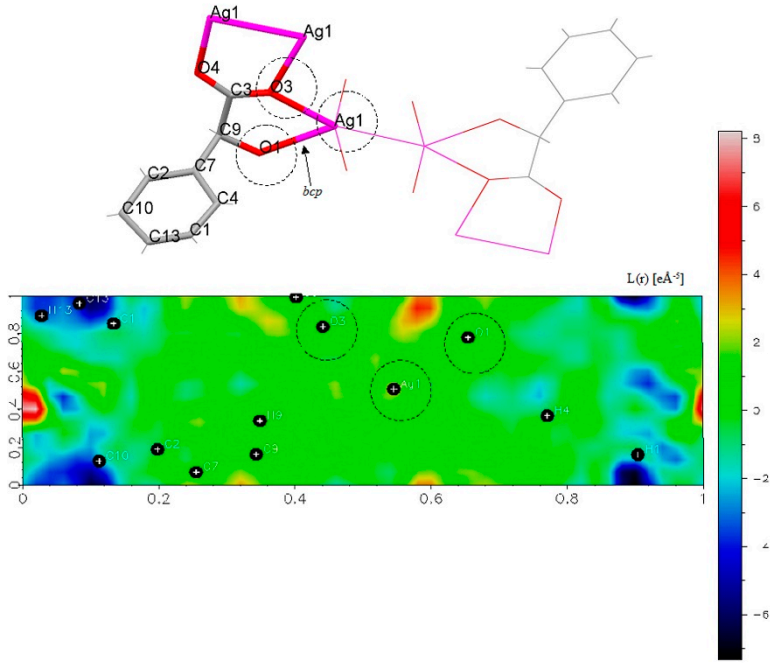

Figure 2. 2D map of Laplacian of electron density $\nabla 2\rho(r)$ [electron.Å^{-5}] of (3); molecular crystallographic structure of (3) and atom labelling scheme. .

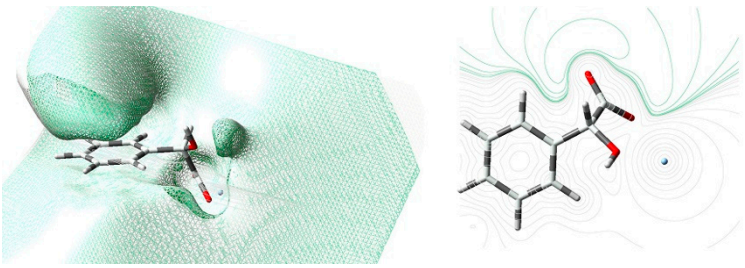

Figure 3. Theoretical (M062X/LANL2DZ) electrostatic potential 2D and 3D maps of (3).

However, the precise determining of both experimentally and theoretically the electron density plays a crucial role in determining the nature of the chemical bonds of the molecules, their energetics, and thus, the properties of molecules and crystals. Owing to the fact that the Hirshfeld surface analysis is broadly utilized for quantifying intermolecular interactions of molecules in crystals it appears clear to us that depending on the accuracy of the data the analysis could be or could not be plausible. Thus, there should be looked for additional criteria for reliable description of the interatomic, respectively, intermolecular interactions of the crystals in order to determine plausibly their energetics and properties.

In looking for such as additional criteria for reliable determining of the nature of the chemical bond and the intermolecular interactions of crystals one inevitably runs among various theoretical approaches assessing the defined quantities via chemometric methods.

Thus, first the current study discusses correlations among crystallographic thermal parameters of atoms in molecules of MA in crystals (1) and (2) (Table S1.) Figure S3 shows linear correlation coefficients between S and eta where the former parameter denotes (isotropic) variance of the mean square amplitude U while eta (η) means correlation coefficient between mutually perpendicular mean-square amplitudes where the latter parameters were defined by Hirshfeld and Shmueli [88]. As can be seen there are obtained |r|=0.98 and 0.892; thus, assuming that the reliability of measurands depends on the quality of the experimental crystallographic datablock of variables and it could vary from measurement-to-measurement. The relative contribution to the discussed parameters such as random experimental and systematic errors; intramolecular vibrations, and more have been

 doi:10.20944/preprints202501.0504.v1

comprehensively detailed on the seminal work [88]. The major research effort which has to do at this point is not only with the accurate processing of the experimental crystallographic datablocks of variables but also with the molecular models which are fitted to the experiment. However, the crystallographic thermal parameters of each atom in the molecules describe, in fact, the fluctuations of the electron density around the average atomic positions. These fluctuations are random, and thus, they unable to be predicted theoretically. Therefore, the crystallographic data provide a statistically averaged molecular structure which fluctuates in time and 3D space. Due to these reasons this study involves both static and molecular dynamics computations of crystals, as well (Figure S4). Furthermore, depending on the complexity of the molecular species in the crystals the motion of the atoms could add anharmonic contribution, as well. The anharmonicity contributes to the systematic error of the molecular model, as well [89]. As can be expected the molecular vibration of crystals is a temperature dependent process. The functional relation has been established by Cruickshank (1956) [90]. Thus, depending on the temperature of the crystallographic measurements there is further variation of the collected datablock of experimental variables of the molecules in the crystals.

Table 1. Experimental crystallographic refinement parameters on crystals**.**

	D,L-MA (polymorph I)	D,L-MA (polymorph I)	D,L-MA (polymorph II)	4-Phenyl-pyridine (bis)mandelate (bis)mandelic acid	catena-((μ3-DL-mandelato)-silver(I))
Compound	(1)			(2)	(3)
CCDC	880481	923825 (P=0.05 GPa)	923830 (P=0.76GPa)	822753	771414
Refs.	[57]	[59]	[59]	This work	[91]
Formula	$C_8H_8O_3$	$C_8H_8O_3$	$C_8H_8O_3$	$C_{27}H_{25}NO_6$	$C_8H_6O_3Ag$
Mr	152.14	152.14	152.14	459.48	258.00
Crystal size	0.48×0.25×0.16	0.44×0.41×0.32	0.42×0.32×0.14	0.47×0.23×0.14	0.53×0.19×0.10
Crystal system	Orthorhombic	Orthorhombic	Monoclinic	Monoclinic	Monoclinic
Space group	Pbca	Pbca	P 2$_1$/c	P2$_1$/n	P2$_1$/c
T [K]	198(2)	296(2)	296(2)	200(2)	300(2)
λ [Å]	0.71073	0.71073	0.71073	0.71073	0.71073
a [Å]	9.9537(15)	9.676(2)	5.825(2)	17.080(3)	16.274(3)
b [Å]	9.6632(15)	16.200(7)	28.908(11)	14.395(3)	4.7421(9)
c [Å]	16.173(3)	9.8866(19)	8.224(6)	19.408(4)	10.3421(19)
α [°]	90.00	90.00	90.00	90.00	90.00
β [°]	90.00	90.00	93.03(4)	96.648(7)	95.093(5)
χ [°]	90.00	90.00	90.00	90.00	90.00
V [Å]	1555.6(4)	1549.74	1382.9	4739.6(16)	795.0(2)
Z	8	8	8	8	4
μ[mm^{-1}]	0.100	0.100	0.113	0.091	2.492
ρ_{calc} [mg.m^{-3}]	1.299	1.304	1.462	1.288	2.156
2θ [°]	25.10	28.36	27.67	25.07	25.03
Refl. collect.	8941	5614	4768	5830	1401
Unique refl.	1386	535	684	614	1107
Obs. refl. [I>2σ(I)]	1386	386	598	614	1401
GOF on F^2	0.796	1.297	1.335	1.359	0.860
R$_1$ [I > 2σ(I)]	0.0410	0.1421	0.2052	0.0632	0.0408
ωR$_2$ (all data)	0.0580	0.2142	0.2242	0.1029	0.0670
Residuals [e.Å^{-3}]	0.119/-0.171	0.110/-0.142	0.281/-0.265	0.446/-0.282	0.696/-1.417

The latter notes are carried out due to the reasons that in most cases the molecular structures of crystals of the same analytes frequently appears to be equated with absence of uncertainty parameters, however, they affect on almost all intermolecular interactions, respectively, molecular

 doi:10.20944/preprints202501.0504.v1

parameters and properties both experimental and theoretical ones. The corresponding atomic coordinates of the molecules in the crystals represent the maximum of the X-ray scattered density fitted of the electron density distribution. It arises due to the molecular structure consisting of atoms providing maximum electron density in the 3D space the thermal displacements. Thus, molecular structure of crystals could be equated only in cases when there are negligible values of the thermal displacement parameters. As Figure S3 reveals the variation can be significant from crystal structure to crystal structure even studying same self-associates as the MA dimers of crystals (1) and (2), because of symmetry operation (–x + 2, –y + 1, –z) generates the whole system of (2). It crystallizes in a monoclinic system and space group type $P2_1/n$ showing unit cell parameters a = 17.080(3), b = 14.395(3), c = 19.408(4) Å, β = 96.648(7)°, Z = 12, V = 4739.6(16)Å3. The crystal structure of (2) was solved by direct methods and refined by full-matrix least-squares on F^2 to final values of R_1 = 0.0667 and wR_2 = 0.1046. In the crystal packing of (2) the species are linked into 3D network via weak intermolecular N+–H···O hydrogen bonds r(N···O)= 2.741, 2.717 Å, between the cations and anions (Figures 1, and S4; Table 1). The anions and the neutral MA molecules form stable self-associates via moderate intermolecular hydrogen OH···O bonds r(O···O)=2.494, 2.535 Å. As in the crystal structure of neutral MA polymorph I (1) two neutral molecules of the acid in (2) form dimer via OH···O bond r(O···O)=2.837 and 2.879 Å. The cationic species exhibit two distinct molecular conformations showing interplanar angles of both the phenyl and pyridinium fragments –27.08° and 1.30° (Figures S5 and S6). The molecular conformations of MA-species in crystals (1)–(3) are summarized in Table S2.

Therefore, despite the available theoretical models connecting between simulated ensembles of molecules in the crystals and the experimental crystallographic data often they cannot count as robust experimental crystallographic practices; furthermore, there can be variation of data within the framework of replicated experiments. Their failure is often grounded to many factors and error contributions as highlighted, above. Due to these reasons in order to obtain some convergence of the view how reliably to draw line between theoretical molecular models and crystallographic experimental data there remains to apply systematically different theoretical approaches complementary; thus, gaining the best theoretical description of experimentally observed phenomena and collected data on molecular systems from perspective of chemometric methods.

Due to these reasons, next, there is presented and discussed experimental and theoretical electron density analysis and energetics of Ag^I-complex of mandelic acid (3). Its crystallographic geometry parameters have already been described [91] together with experimental electron spectroscopic and vibrational spectra [57]. Briefly, the AgI-ion of dinuclear Ag^I-containing sub-structure is connected with four O-atoms, having bond Ag–O distances within r(Ag···O)=2.215–2.492 Å (Figure S7). The interionic Ag^I–Ag^I interaction has distance r(Ag···Ag)=2.820 Å. The MA anion acts as a tridentate ligand via deprotonated COO- and OH-groups. The carboxylate anion COO^- is bonded to two Ag^I-ions in a dinuclear sub-unit. The OH-group appears bridged ligand center coordinating each of binuclear cores; thus, forming coordination polymer. The geometry of Ag^IO_5 metal chromophore is distorted trigonal pyramidal structure. With these considerations in mind this study specifies practical utilization of experimentally measured crystallographic variable and their complementary treatment with theoretical quantum chemistry data; thus, presenting and discussing novel data on (3) for purposes of determining and predicting molecular properties and energetics from crystallography. This line of research is particularly strengthened if there is considered experimental and theoretical electron density (ED) values of atoms in the molecule of (3). The real ED values of atoms in molecules within the 3D space is determined using least square refinement ED parameter ED ρ(r) (Figure S2) [92]. The F_o-maps reflect experimental ED at each point of the 3D space. In addition to 2D ED distribution, there is 3D ED one.

Thus, there are evaluated rho(r) (or ρ(r)) and Laplacian_rho(r) (or L(r)) of experimental ED of atoms in the molecules (Figure 2). The electrostatic potential surface of (3) and M062X/LANL2DZ level of theory is depicted in Figure 4. The developed theories of knowledge of nature of interatomic interactions in molecules or metal-to-ligand coordination of Ag^I-ion with O-center from MS via crystallography import reliable statistical assessment of ρ(r) and L(r) values between interacting

 doi:10.20944/preprints202501.0504.v1

species. Thus, when there is predominating ionic M–L interactions, then rho(r) values are within the 0.2–0.3 eÅ^{-3} [93]. In cases when rho(r)>0.6 e Å^{-3} there is predominantly covalent M–L bond. Owing to the fact that there is statistical assessment of uncertainty of experimental crystallographic datasets of variables the reliability of absolute quantification of experimental ED of atoms or rho(r) data on, depends on reliability of Laplacian_rho (r). It is determined using experimental crystallographic factors reflecting completeness of the so-called Fourier series, and Fourier amplitudes' quality in addition to and model applied to ED distribution [94].

Therefore, the reliability of rho(r) and Laplacian_rho(r) data are connected with quality of data collection of hkl reflections and applied refinement model. Regarding, quality of data-blocks of measurable variables there should be mentioned important factors such as resolution of crystallographic measurements, quality of single crystalline object, and it scattering properties. There are permanent random errors of crystallographic measurements which are result from fluctuation of atomic vibration factors, as well. Due to these reasons, our knowledge of nature of intermolecular interactions including metal-to-ligand ones obtained via crystallography are reliable and correct ones, but they cannot be regarded as absolute knowledge, because of in fact, rho(r) is a probability function of experimental ED, as aforementioned. It is not an absolute quantity of ED at point (x,y,z) of the 3D space. Therefore, absolute assignment of nature of neither M–L bonds nor intermolecular hydrogen bonding interactions or short contacts cannot be achieved even processing high quality crystallographic data-blocks of variables. The developed theories also implies that Laplacian_rho(r) (and gradient_rho(r)) reflects the so-called bond paths or boundaries of interacting species [95–103]. The implementation of charge density models allow for evaluating via quantitative criteria realistic of inter-atomic, respectively, intermolecular interactions of crystals. From this theoretical perspective interacting species are described as chemically bonded when there are different (3,-1) so-called bond critical points in rho(r) between them [102]. When Laplacian_rho(r) values < 0, then there is charge concentration. A Laplacian_rho(r) > 0 means charge depletion. The Laplacian_rho(r) is given by a sum of λ_i parameters. The parameter ellipticity (ε) details on bond order of interactions. When there is σ-bond, then λ_1–λ_2 cause for bond critical point (bcp) = 0 because of λ_1 and λ_2 are mutually perpendicular to chemical bond axes within cylindrical symmetry approximation along bond axis. The increasing in bond order causes for increasing in ellipticity. The results from crystal (3) (Table 2) show ε=0.0170 and 0.0067 of Ag^{I}-O1 and Ag^{I}-O3 interactions. The values are relatively large comparing with purely ionic interactions [91]. Thus, there can be proposed a charge de-localization. The latter experimental data are correlated with theoretical natural ionicity parameter (i_{AB}) determined according to equation (S1) [97]. It is calculated using the M062X/LANL2DZ natural polarization coefficients (c_A, c_B) obtained of (3) and summarized in Table S3. As can be seen there is calculated $i_{Ag\text{-}O1}$=-0.0544, which confirms the crystallographic results; thus, indicating a charge de-localization effect. The latter value is significantly high comparing with $i_{Zn\text{-}Cl}$ one of -0.76 determined of $ZnCl_4^{2-}$ counter ion containing crystals of coordination compounds [104]. The latter species are characterized with almost purely ionic Zn-Cl bond and ionic hybrid localized at the Cl^- centers. The C–O bonds of MA of (3) show $i_{C\text{–}O}$ =0.4386–0.1853.

Further, effort in development of crystallographic based approaches to detail on nature of interatomic, respectively, intermolecular interactions of molecules and their ensembles of crystals has given and adequate account of relation between interaction energy and rho(r) at the bcp which is approximated linearly [91,104]; thus, stressing on important correlation between characteristic of M–L bond and energy of interactions. Among models connecting between experimental crystallographic ED electron densities, expressed by Laplacian as shown above and energy terms, there can be highlighted the Abramov's model equation (1) [103,105]. The G(r) denotes electronic kinetic energy. The V(r) means potential energy at bcp. The latter model is used to study complex (3) (Table 3,) because of within a series of Ag^{I}-, Cu^{II}-, and Zn^{II}-complexes of organics there has been found that V(r) depends linearly from the theoretically obtained dissociation energy D_{i0} of i^{th} chemical bond of molecules of crystals [91,104,106].

 doi:10.20944/preprints202501.0504.v1

$$\frac{1}{4}\nabla^2\rho = 2G(r) + V(r) \quad (1)$$

Due to these reasons, this study treats functional relation V(r)=f(D^{i}_{0}) of Ag^{I}-complex of MA (3), as well. The correlative analysis between experimental crystallographic bond energy parameters according to equation (1) of V(r) listed in Table 3 and theoretical Di0 parameters as determined in Figure S8 as well as M062X/LANL2DZ energetics of species (Table S4) yields to excellent performances, showing |r|=0.9999 (Figure 4(A).) Therefore, theoretical bond dissociation energy parameters and V(r) potential energy of bonds at bcps according to equation (1) allow for reliable correlation between theoretical and experimental crystallographic properties and energetics of molecules in crystals.

Owing to the fact that the experimental and theoretical design of the study is governed by the so-called means-end reasoning, further, it concentrates on determining of Hirshfeld atomic charges and populations which are essential for modeling of physico-chemical properties of molecules, as aforementioned (Tables S5 and S6). There are listed the ESPs, as well. The correlative analysis between Hirshfeld atomic charges and populations of (3) shows |r|=0.7007 (Figure 4(B)).

Since, a particular focus on this study is on accurate tools for theoretical and experimental description and prediction of atomic, respectively, molecular interactions of crystals, it should be highlighted that the tabulated Hirshfeld population analysis can be used for exact determining of molecular dipole moments and higher multipole ones.

However, often one needs relatively simple representation of the charge re-distribution of the molecules using only atomic charges or the so-called monopole approximation. This is the case, for instance, when there is mapped the Hirshfeld charges on a novel set of charges reliably representing the ESPs, but without to account for atomic dipoles, because of ESPs predicts accurately the chemical reactivity of the molecules [86]. For the latter purposes this study uses also the Truhlar's charge models called CM5 [107]. The correlation between Hirshfeld and CM5 charges shows |r|=0.98531.

However, the correlative analysis between Hirshfeld charges or CM5 charges and ESPs of (3) yields to |r|=0.1791 (Figure 4(C)). The low performances are due to deviation of ESP value of Ag^{I}-ion, because of there is coefficient of linear correlation |r|=0.99561 of the same data when there is excluded from the ESP value of the metal ion. The latter rather controversial data are explained with the fact that in the complex (3) there is charge de-localization as both crystallographic and theoretical natural bond orbital analysis data have shown, above.

Therefore, the metal-to-ligand charge de-localization effect of ^{AgI}-complexes should be tackled using complementary both ESP and atomic charges, respectively, electron densities, but also natural polarization coefficients, thus allowing for an in-depth characterizing of the nature and energetics of the coordinative metal-to-ligand bond. Due to reasons presented, herein, it seems that the complementary employment in the later approaches is more useful to study reliably the physico-chemical properties of molecules in the crystals.

Preprints.org (www.preprints.org) | NOT PEER-REVIEWED | Posted: 7 January 2025 doi:10.20944/preprints202501.0504.v1

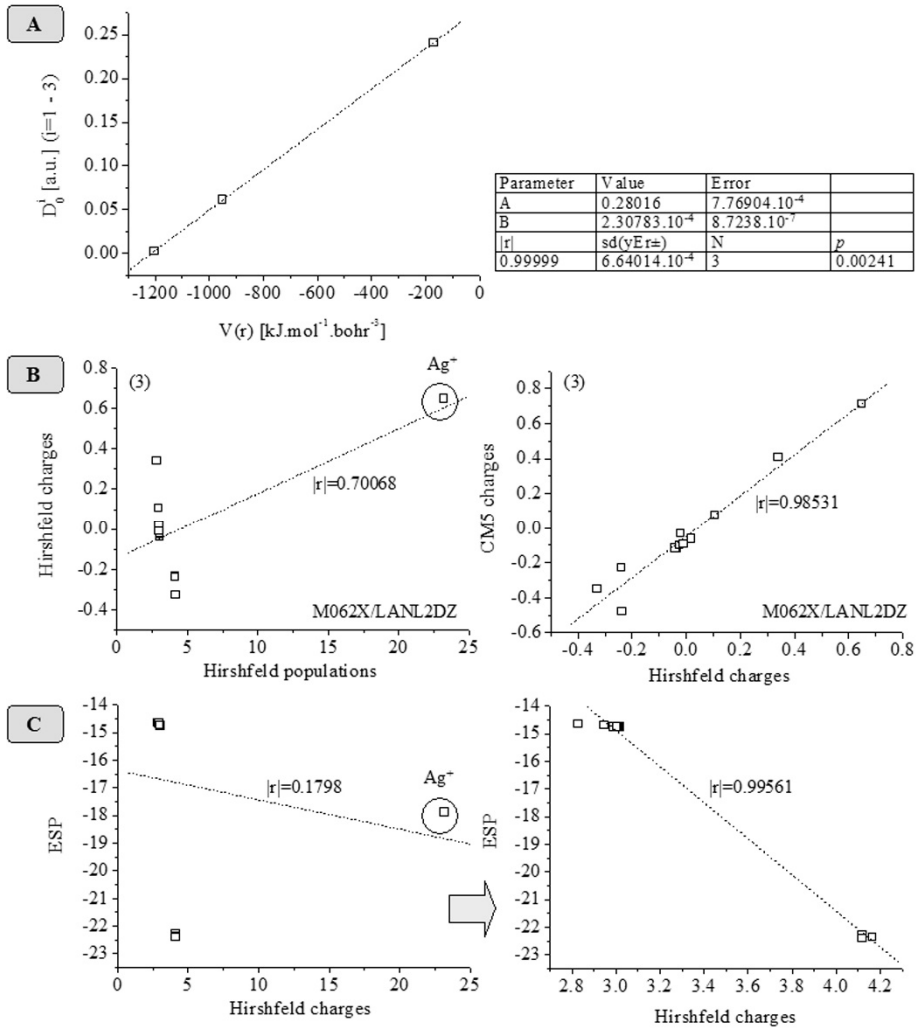

Figure 4. Functional relations between theoretical bond dissociation energy data on (3) (D^{i}_{0} [a.u.]) as defined in Figure S8 (Table S4) and experimental crystallographic data on V(r) [kJ.mol^{-1}.Bohr^{-3}] (Table 3) (A); Hirshfeld charges and populations as well as CM5 charges (Tables S5 and S6) (B); and Hirshfeld charges and electrostatic potentials (Table S6) (C); chemometrics.

Table 2. Bond critical point analysis of crystals of compound (3); the Laplacian of electron density $\nabla^2\rho(\mathbf{r})$ [electron.Å^{-5}]; electron density $\rho(\mathbf{r})$ [electron. Å^{-3}]; λ_i – parameters (i = 1–3) ($\nabla^2\rho(\mathbf{r}) = \lambda_1 + \lambda_2 + \lambda_3$); intermolecular saddle (3,-1) critical points are described; the interactions with H-atoms are omitted; atom labelling scheme (**Figure 2**).

Atom_1	Atom_2	ρ(r)	∇²ρ(r)	λi, i = 1–3			Ellipticity (ε)
				λ1	λ2	λ3	
Ag1	O1	0.2411	4.00	-0.92	-0.90	5.82	0.0170
Ag1	O3	0.2068	3.34	-0.74	-0.74	4.81	0.0067
O1	C9	1.4501	4.42	-7.60	-7.59	19.61	0.0012
O3	C3	1.8884	-3.23	-9.74	-9.59	16.09	0.0154
O4	C3	2.0915	3.83	-11.08	-10.91	25.82	0.0154
C1	C4	1.4311	-1.35	-6.71	-6.44	11.80	0.0412
C1	C13	1.7817	-7.35	-8.55	-8.27	9.47	0.0346
C2	C7	1.4228	-1.34	-6.67	-6.41	11.74	0.0402

 doi:10.20944/preprints202501.0504.v1

C2	C10	1.5170	-2.72	-7.18	-6.93	11.40	0.0359
C3	C9	1.2828	0.39	-5.79	-5.78	11.95	0.0024
C4	C7	1.4939	-2.39	-7.05	-6.80	11.47	0.0368
C7	C9	1.3293	-0.10	-6.07	-5.95	11.92	0.0198
C10	C13	1.3169	0.07	-6.09	-5.83	11.99	0.0448

Table 3. Topological energetics of complex (3) using experimental electron densities; G_{cp} – Kinetic energy at bcp [a.u.Bohr^{-3}]; V_{cp} – Potential energy at bcp [a.u./bohr^{-3}] or [kJ.mol^{-1}.bohr^{-3}]; intermolecular saddle (3,-1) critical points are described; the interactions with H-atoms are omitted; atom labelling scheme (**Figure 2**).

Atom_1	Atom_2	G_{cp}	V_{cp}	G_{cp}	V_{cp}
		[a.u.Bohr^{-3}]	[a.u.Bohr^{-3}]	[kJ.mol^{-1}.Bohr^{-3}]	[kJ.mol^{-1}.Bohr^{-3}]
Ag1	O1	0.03878	-0.03608	101.82	-94.73
Ag1	O3	0.03170	-0.02878	83.22	-75.55
O1	C9	0.25190	-0.45797	661.35	-1202.40
O3	C3	0.32141	-0.67633	843.87	-1775.71
O4	C3	0.43401	-0.82829	1139.49	-2174.68
C1	C4	0.20722	-0.42842	544.05	-1124.81
C1	C13	0.26115	-0.59855	685.65	-1571.50
C2	C7	0.20519	-0.42428	538.72	-1113.94
C2	C10	0.21980	-0.46783	577.08	-1228.30
C3	C9	0.18313	-0.36224	480.80	-951.06
C4	C7	0.21610	-0.45694	567.36	-1199.69
C7	C9	0.19078	-0.38259	500.90	-1004.48
C10	C13	0.18903	-0.37729	496.30	-990.57

2.2. Vibrational Spectroscopic Data

Owing to the fact that the vibrational spectroscopy [108–110] is routinely implemented as a robust tool for structural analysis of solids including crystals in the pharmaceutical industry Figures 5, S9, and S10 depict experimental solid-state and theoretical (M062X/LANL2DZ) IR-spectra of crystals (2) and (3). The vibrational modes of both the IR and Raman active ones of racemate and enantiopure forms of the former analyte have been comprehensively detailed on theoretically and experimentally [108]. The IR-spectrum of (1) is detailed on [57].

The IR-spectrum of (2) shows ν_{OH} stretching vibration at 3460 cm^{-1} assigned to MS structural sub-unit. The $\nu_{C=O}$ stretching vibration is observed at 1695 cm^{-1}. The low-frequency shifting of the mode comparing with the data on (1) and those ones reported previously [108] at 1714 cm^{-1} is result from experimentally determined shorter C-O bond of the acid in crystals of (2) exhibiting bond lengths within r(C–O)=1.236–1.259 Å while the corresponding data on (1) is r(C=O)=1.207 Å.

Despite the fact that there is deprotonated COOH-fragment of MA in the former crystal there are asymmetric intermolecular interactions causing or distortion of local C_{2v} symmetry of carboxylate anionic structural sub-unit. The strongly intensive IR-band at 693.069±0.53 cm^{-1} belongs to out-of-plane bending vibration of mono-substituted phenyl fragment of MA. As can be expected, there is difference in $\Delta\nu$=|2| cm^{-1} comparing with results from pure MA racemate. The latter results agree well with those one reported to work [108] showing a value of 695 cm^{-1}. The strong intensive bands at 764.64±0.3 and 727.64±0.25 cm^{-1} belong to 4-phenyl-pyridinium counter ion.

Despite the fact that the IR-spectroscopy is broadly implemented as aforementioned into the field of pharmaceutical industry as reliable tool for structural analysis of multicomponent pharmaceutical formulations, including those ones of MA [109] the IR-pattern could be very

 doi:10.20944/preprints202501.0504.v1

complicated (Figure 5(C).) As the curve-fitted spectrum of (2) in the latter figure reveals there is a set of stretching $\nu_{C=O}$ and $\nu^{as}_{COO^-}$ vibrations within 1800–1500 cm^{-1} region due to presence of both neutral MA and its anion in the crystal of (2). A comprehensive vibrational analysis of co-crystals and salts of MA via IR-spectroscopy [109] has assigned the IR-band at 1732 cm^{-1} to $\nu_{C=O}$ stretching vibration of S-MA enantiomer, while the band at 1704 cm^{-1} to $\nu_{C=O}$ mode of R-MA enantiomer. The band at 1669 cm^{-1} has been assigned to ν_{COO^-} mode. The comparative analysis of IR-spectra of crystals of (2) and (3) in this study both containing MA anion, however, show intensive IR-band at 1616 cm^{-1} in the former crystal assigned theoretically to $\nu^{as}_{COO^-}$ stretching vibration. The same mode is shifted to 1561 cm^{-1} in (3) due to coordination of the MA-anion with Ag^{I}-ion. The observed shifting of $\Delta|n|$=55 cm^{-1} (Figure 5(B)) further support the crystallographic and theoretical electron density data and natural ionicity parameters showing that the Ag–O bonds of (3) are characterized with significant charge de-localization; thus, lacking of purely ionic interactions of species MA-COO- and Ag^{+} species which is typically observed in Zn^{2+} complexes with chalcogenide ligands [104].

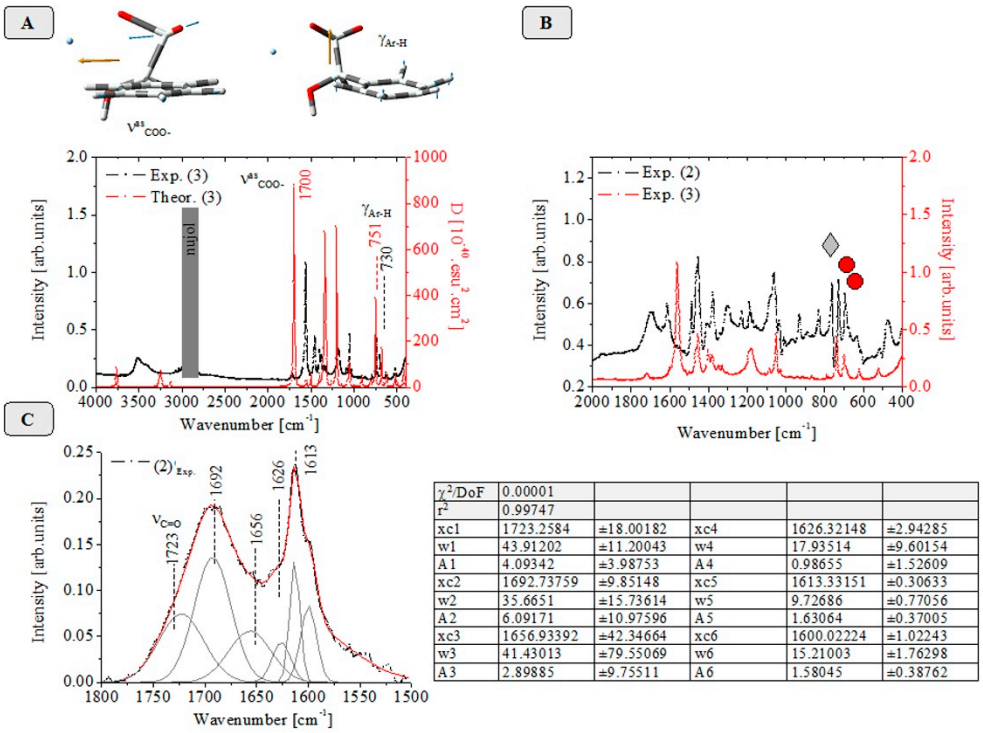

χ^2/DoF	0.00001				
r^2	0.99747				
xc1	1723.2584	±18.00182	xc4	1626.32148	±2.94285
w1	43.91202	±11.20043	w4	17.93514	±9.60154
A1	4.09342	±3.98753	A4	0.98655	±1.52609
xc2	1692.73759	±9.85148	xc5	1613.33151	±0.30633
w2	35.6651	±15.73614	w5	9.72686	±0.77056
A2	6.09171	±10.97596	A5	1.63064	±0.37005
xc3	1656.93392	±42.34664	xc6	1600.02224	±1.02243
w3	41.43013	±79.55069	w6	15.21003	±1.76298
A3	2.89885	±9.75511	A6	1.58045	±0.38762

Figure 5. Theoretical (M062X/LANL2DZ) and experimental solid-state infrared spectra of (2) and (3) within the different regions of the electromagnetic spectrum; visualization of selected theoretically obtained molecular vibrations of (3) (A,B); curve-fitted experimental IR-pattern of (2) using Gauss/Lorentz mixed function at ratio 1:1; chemomerics. .

2.3. UV-VIS-NIR Data

Figure 6 depicts theoretical and experimental EOM-CCSD data on MA and crystals (1)–(3). The theoretical data are detailed on Table S7. As an effort to account for charge transfer effects of the species there is used computation of long range transition densities, as well. A difference between theoretical and experimental absorption maxima $\Delta|\lambda_{max}|$=10 nm is obtained. The experimental data on MA agree well with previously reported study of MA in aqueous solution showing λ_{max}=218 nm, assigned to n→π* transition [111]. Thus, the experimental data on crystal (2) showing λ_{max}=269 and 290 nm indicates that these bands belong to n→π* and π→π* transitions of the protonated cation, while the intensive band at λ_{max}=225 nm of (3) is assigned to charge transfer one due to coordination of MA with Ag^{I}-ion. An important remark on the latter assignment, however is that the complex (3) is unstable in solution. Its mass spectrometric analysis has been detailed on [112]. The Ag^{I}-ion

 doi:10.20944/preprints202501.0504.v1

preferably forms solvate complexes. There are observed only low abundance MS peaks at m/z 278.04 and 280.04 of $^{107/109}$Ag complex of MA (Figure S11). Thus, I shall conclude the experimental description of the electronic absorption properties of (3) with the highlight that there could be failure assigning experimental spectra of crystals in solution because of there should be carried our correlation of electronic absorption properties of various processes particularly highlighting coordination compounds where competitive ligand exchange of solvent molecules is frequently occurred.

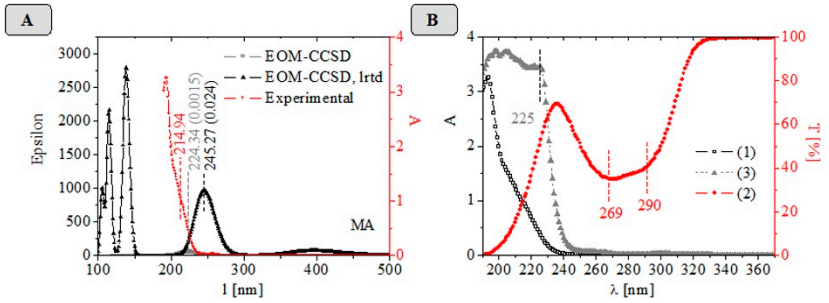

Figure 6. Theoretical equation-of-motion coupled cluster with single and double substitutions (EOM-CCSD) spectra of mandelic acid together with its experimental electronic absorption spectrum in CH_3OH (A); experimental electronic absorption and transmission spectra of crystals (1)–(3) in CH_3OH (B). .

3. Discussion

To begin with, observational facts about molecular systems and their interacting ensembles via methods of chemical crystallography generate our experimental or empirical knowledge not only of the 3D molecular structure of the matter together with geometry parameters of the molecules such as bond lengths and angles, but also properties of the matter and the energetics of the molecular systems, including the chemical bonds of the molecules. As far as there is correct functional dependence between the energetics of the molecular ensembles of interacting species in crystals and the property of the matter including its biological activity as has been described in the preceding sub-sections of this study, then, the experimental crystallographic knowledge of the molecular crystals provides direct link between the molecular structure and biological function which is of utmost importance for the field of pharmaceutical industry and medicine where the commercially distributed pharmaceutics formulations via salt crystallization processes modulate the solubility of the active ingredient and its pharmacological effect. Owing to the fact that the salt formulation is among the most utilized strategy for improving properties of medications is routinely implemented into pharmaceutical industry; thus, producing free therapeutics forms via process of disproportionation the reliable description of energy parameters of crystals are of significant importance for the salt crystallization screening of therapeutics and their implementation into the clinical practice. The major motivation behind the latter statement is the fact that the process of disproportionation is thermodynamically and kinetically driven one. Thus, thought mainly crystallographic experiment alone the latter lines of research there could be generated reliable knowledge of properties of analyte crystals and their biological function; if any. The same is valid to vibrational spectroscopy which is routinely implemented approach to determine multicomponent solids and crystals for the purposes of the pharmaceutical industry.

However, even if a molecular system is well characterized or determined thought experimental methods as aforementioned ones there is impossible to bring directly the experimental knowledge of the energetics of the molecules and crystals. Therefore, the experimental datasets of variables of molecular systems and crystals are not very informative themselves about neither geometry parameters of molecules nor their properties or energetics. In fact the theory and model equations processing experimental data on molecular systems tell us something about the molecular structure

 doi:10.20944/preprints202501.0504.v1

and the property of the matter including its energy. Due to these reasons testing of theories and model functional relations against experimental data tell us anything reliably about the matter and its properties. At this point we take advantage mainly on well-supported experimental knowledge in order to convince first ourselves that the conducted experiment is produced reliable and justified empirical knowledge of the molecular systems and their thus, proposed biological function. Despite the fact that the current discussion only grasped the surface of how to assess via experiment molecular properties and energetics of the matter it aims at highlighting that our systematic correlative analysis between experimental crystallographically determined energetics of chemical bonds of molecules in crystals and the theoretically determined bond dissociation energy of the modes of molecular systems using the Abramov's equation (1) provides pretty easy and highly reliable information about the energetics of the molecular systems in the crystals thought crystallographic experiment [104,106]. This study, has reported first the best chemometric performances of the latter relationship showing up to $|r|=0.9999$ and studying Ag^{I}-complex of mandelic acid. Therefore, thought experimental crystallographic data as a form of generating empirical claim or this is our knowledge from the experiment of the matter there is known the energetics of the molecular systems. This represent the traditional point of view of the experimental science. However, this claim does not seem to be neither completely precise nor objective one nor to be general claim. Rather, this study provides novel pro-argument about the statement that the most accurate theoretical model processing experimental crystallographic data is only capable of generating reliable empirical claim and knowledge of the mater and its properties, because of we cannot observed directly the mass of the matter and elementary particles of molecular species in crystals. The excellent performances achieved in this paper, however, suggest that equation (1) best describes the experimental energetics of the chemical bonds of the molecules; and thus, it can be applied to obtain reliable conclusive statements regarding the molecular properties of the mandelic acid crystals.

4. Materials and Methods

(Consider supporting information)

5. Conclusions

The final conclusions are drawn about the following crystals of mandelic acid:

(A) First, in this study there is reported crystal structure of 4-phenyl-pyridinium mandelate mandelic acid (2). The symmetry operation (–x + 2, –y + 1, –z) generates the whole system, which crystallizes in a monoclinic system and space group type P21/n showing unit cell parameters a = 17.080(3), b = 14.395(3), c = 19.408(4) Å, β = 96.648(7)°, Z = 12, V = 4739.6(16) $Å^3$. The crystal structure was solved by direct methods and refined by full-matrix least-squares on F^2 to final values of R_1 = 0.0667 and wR_2 = 0.1046. There is performed experimental and theoretical electron density analysis, as well. The infrared vibrational spectroscopic and electronic absorption properties of (2) are reported and described both experimentally and theoretically.

(B) The novel data on experimental and theoretical electron density analysis of crystals of Ag^{I}-complex of mandelic acid correlating between crystallographic potential energy data on bond critical point according to Abramov's model and theoretical bond dissociation energy yields to the best method performances, showing $|r|=0.9999$. The tool seems that best characterizes experimental crystallographic energetics of chemical bonds of molecules fitted off high accuracy methods of quantum chemistry.

Supplementary Materials: The following supporting information can be downloaded at the website of this paper posted on Preprints.org, There is experimental and theoretical structural, thermochemical, and molecular spectroscopic parameters of crystals (Figures S1–S14 and Tables S1–S7), CCDC 822753 (2) contains supplementary crystallographic data for the crystals. The crystallographic information files can be obtained free of charge via http://www.ccdc.cam.ac.uk/conts/retrieving.html or from Cambridge Crystallographic Data

 doi:10.20944/preprints202501.0504.v1

Centre, 12 Union Road, Cambridge CB2 1EZ, UK; fax: (+44) 1223-336-033; or e-mail: deposit@ccdc.cam.ac.uk. Supplementary data associated with this paper can be found, in the online version.

Author Contributions: B.I. contributes to conceptualization; methodology; software; validation; formal analysis; investigation; resources; data curation; writing—original draft preparation; writing—review and editing; visualization; supervision; project administration; and funding acquisition. All authors have read and agreed to the published version of the manuscript.

Funding: Not applicable.

Data Availability Statement: Experimental raw files and theoretical output ones used to this study can be downloaded free of charge [https://doi.org/10.5281/zenodo.14601517].

Acknowledgments: The author is grateful to Deutscher Akademischer Austausch Dienst for the domation of Evolution 300 UV-VIS-NIR spectrometer; the Alexander von Humboldt Stiftung for the grant and the donation of single crystal X-ray diffractometer for laboratory of "Molecular Spectroscopy and Structural Analysis" at Department of Analytical Chemistry at Sofia University "St. Kl. Ohridski"; the Deutsche Forschungsgemeinschaft; and the central instrumental laboratory clusters of mass spectrometry at the Institute of Environmental Research at the Dortmund University of Technology.

Conflicts of Interest: The author declares no conflicts of interest.

References

1. Euldji, I.; Si-Moussa; Hamadache, M.; Benkortbi, O. QSPR modelling of the solubility of drug and drug-like compounds in supercritical carbon dioxide. *Mol. Inf.* **2022**, *41*, 2200026.
2. Kumari, N.; Ghosh, A. Cocrystallization: Cutting edge tool for physicochemical modulation of active pharmaceutical ingredients. *Curr. Pharmaceut. Des*. **2020**, *26*, 4858-4882.
3. Duggirala, D., Perry, M.; Almarsson, Ö.; Zaworotko, M. Pharmaceutical cocrystals: along the path to improved medicines. *Chem. Commun. (Camb)* **2016**, *52*, 640-655.
4. Almarsson, O.; Zaworotko, M. Crystal engineering of the composition of pharmaceutical phases. Do pharmaceutical co-crystals represent a new path to improved medicines? *Chem. Commun. (Camb)* **2004**, (*17*), 1889-96.
5. Shah, H., Michelle, C., Xie, T., Chaturvedi, K., Kuang, S., Abramov, Y. Computational and experimental screening approaches to aripiprazole salt crystallization. *Pharmaceut. Res*. **2023**, *40*, 2779-2789.
6. [https://www.future-marketinsights.com/reports/oral-solid-dosage-pharmaceutical-formulation-market]
7. Tan, Q., Hosseini, S., Thévenin, D. In Nagel, W., Kröner, D., Resch, M- (Eds.), Chapter: Simulations of crystal growth using lattice Boltzmann formulation, High Performance Computing in ccience and engineering '22. Springer Nature Switzerland AG 2024, pp. 387-475.
8. Tan, Q., Hosseini, S., Seidel-Morgenstern, A., Thévenin, D., Lorenz, H. Thermal effects connected to crystallization dynamics: A lattice Boltzmann study. *Int. J. Multiphase Flow* **2024**, *171*, 104669.
9. Nechipadappu, S., Swain, D. New drug-drug and drug-nutraceutical salts of anti-emetic drug domperidone: structural and physicochemical aspects of new salts. *CrystEngComm*, **2024**, *26*, 926-942.
10. Zhou, J., Wei, Y., Wu, J., Li, S., Xu, Z., Peng, Y. Novel ethylenediamine-β-cyclodextrin grafted membranes for the chiral separation of mandelic acid and its derivatives. *Chirality*. **2024**, *36*, e23662.
11. Tenorio, J., Alves, D., Carvalho Jr. P. Diastereoisomeric double salts of carvedilol with (L)- and (D)-mandelic acids. *J. Mol. Struct.* **2025**, *1325*, 140909.
12. De Meester, J., Layrisse, P., Marchivie, M.; Collard, M., Wery, G., Brandel, C., Cartigny, Y., Subra-Paternault, P., Leyssens, T., Harscoat-Schiavo, C. Towards a new approach in chiral resolution: Pressurized-CO_2 assisted preferential cocrystallization. *J. Supercriti. Fluids* **2024**, *212*, 106339.
13. Martínková, L., Křen, V. Biocatalytic production of mandelic acid and analogues: A review and comparison with chemical processes. *Appl. Microbiol. Biotechnol*. **2018**, *102*, 3893-3900.
14. Li, J., Cosler, L., Harausz, E., Myers, C., Kufel, W. Methenamine for urinary tract infection prophylaxis: A systematic review. *Pharmacotherapy*. **2024**, *44*, 197-206.
15. Fitriani, L.; Fadina, H.; Usman, H.; Za, Z. Information and characterization of multicomponent crystal of triamethoprim and mandelic acid by solvent drop griding method. *Int. J. Appl. Pharmaceut*. **2023**, *15*, 75-79.

 doi:10.20944/preprints202501.0504.v1

16. Songsermsawad, S.; Nalaoh, P.; Promarak, V.; Flood, A. Chiral resolution of RS-baclofen via a novel chiral cocrystal of R-baclofen and L-mandelic acid. *Cryst. Growth Des*. **2022**, *22*, 2441-2451.
17. Trawally, M.; Demir-Yazici, K.; Birgül, S.; Kaya, K.; Akdemir, A.; Güzel-Akdemir, O. Mandelic acid-based spirothiazolidinones targeting *M. tuberculosis*: Synthesis, in vitro and in silico investigations. *Bioorg. Chem*. **2022**, *121*, 105688.
18. Vimalson, D; Parimalakrishnan, S.; Jeganathan, N.; Anbazhagan, S. Techniques to enhance solubility of hydrophobic drugs: An overview. *Asian J. Pharm*. **2016**, *10*, S67-75
19. Chen, W.; Qiu, X.; Chen, Y.; Ke, J.; Ji, Y.; Chen. J. Supramolecular interaction modulation in thermosensitive composites: Enantiomeric recognition and chiral site regeneration. *Anal. Chem*. **2024**, *96*, 5580-5588.
20. Zhang, Y.; Su, C.; Lei, J.; Chen, L.; Hu, H.; Zeng, S.; Yu, L. Studies on the L-2-hydroxy-acid oxidase 2 catalyzed metabolism of S-mandelic acid and its analogues. *Drug Metabol. Pharmacokinet*. **2019**, *34*, 187-193.
21. Tay, H.; Hua, C. Chiral coordination polymers of mandelate and its derivatives: Tuning crystal packing by modulation of hydrogen bonding. *Aust. J. Chem*. **2022**, *75*, 94-101.
22. Zhou, F.; Shemchuk, O.; Charpentier, M.; Matheys, C.; Collard, L.; Ter Horst, J.; Leyssens, T. Simultaneous chiral resolution of two racemic compounds by preferential cocrystallization. *Angew. Chem. Int. Ed*. **2021**, *60*, 20264-20268.
23. Wang, J.; Peng, Y. Resolution of halogenated mandelic acids through enantiospecific co-crystallization with levetiracetam. *Molecules* **2021**, *26*, 5536.
24. Zhou, F.; Body, C.; Robeyns, K.; Leyssens, T.; Shemchuk, O. On the pairwise cocrystallization of racemic compounds. *CrystEngComm* **2023**, *25*, 3060-3065.
25. Zahoor, M.; Shafiq, S.; Ullah, H.; Sadiq, A.; Ullah, F. Isolation of quercetin and mandelic acid from Aesculus indica fruit and their biological activities. *BMC Biochemistry* **2018**, *19*, 5.
26. Guo, Q.; Li, Y.; Shi, H.; Yi, A.; Xu, X.; Wang, H.; Deng, X.; Wu, Z.; Cui, Z. Novel mandelic acid derivatives suppress virulence of *Ralstonia solanacearum* via type III secretion system. *Pest Manag Sci* **2023**, *79*, 4626-4634.
27. Sun, Z.; Ning, Y.; Liu, L.; Liu, Y.; Sun, B.; Jiang, W. Metabolic engineering of the L-phenylalanine pathway in *Escherichia coli* for the production of S- or R-mandelic acid. *Microb. Cell Fact.* **2011**, *10*, 71.
28. Zhang, Y.; Wang, X.; Shi, H.; Siddique, F.; Xian, J.; Song, A.; Wang, B.; Wu, Z.; Cui, Z. Design and synthesis of mandelic acid derivatives for suppression of virulence via T3SS against Citrus canker. *J. Agric. Food Chem*. **2024**, 72, 9611-9620.
29. Sklyarenko, A.; Groshkova, I.; Gorbunov, N.; Vasiliev, A.; Kamaev, A.; Yarotsky, S. Comparative evaluation of the effectiveness of biocatalytic synthesis and antibacterial activity of known antibiotics and "chimeric" cephalosporin compounds. *Appl. Biochem. Microbiol*. **2024**, *60*, 431-438.
30. Bhavsar, S.; Tadiparthi, R.; Gupta, S.; Pawar, S.; Yeole, R.; Kayastha, A.; Deshpande, P.; Bhagwat, S.; Patel, M. Design and development of efficient synthetic strategies for the chiral synthesis of novel ketolide antibiotic, nafithromycin (WCK 4873). *Chem. Pap.* **2023**, *77*, 3629-3640.
31. Chen, J.; Lv, Q.; Tu, G. Synthesis and molecular simulation studies of mandelic acid peptidomimetic derivatives as aminopeptidase N inhibitors. *Curr. Comp.-Aid. Drug Des*. **2021**, *17*, 619-626.
32. Aslani, S.; Armstrong, D. Fast, sensitive LC–MS resolution of α-hydroxy acid biomarkers via SPP-teicoplanin and an alternative UV detection approach. *Anal. Bioanal. Chem.* **2024**, *416*, 3007-3017.
33. Widgerow, A.; Ziegler, M.; Garruto, J.; Ionescu, L.; Shafiq, F.; Meckfessel, M.; Lain, E.; Ablon, G.; Harper, J.; Chang, A.; Howard-Verovic, C. Novel strategy for strengthening dermatoporotic skin by managing cellular senescence. *J. Drugs Dermatol.* **2024**, *23*, 748-756.
34. Duan, Q.; Ye, Z.; Zhou, K.; Wang, F.; Lian, C.; Shang, Y.; Liu, H. An investigation into the transdermal behavior of active ingredients by combination of experiments and multiscale simulations. *J. Phys. Chem. B* **2024**, *128*, 6327-6337.
35. Kopple, J. Phenylalanine and tyrosine metabolism in chronic kidney failure. *J. Nutr.* **2007**, *137*, 1586S-1590S.
36. Bocato, M.; Quero, R.; Weil,A.; Cesila, C.; Adeyemi, I.; Barbosa Jr. F. A new adsorptive 3D–printed sampling device for simultaneous determination of 63 urinary organic acids by LC–MS/MS. *Anal. Chim. Acta* **2024**, *1288*, 342185.

 doi:10.20944/preprints202501.0504.v1

37. Yevglevskis, M.; Bowskill, C.; Chan, C.; Heng, J.; Threadgill, M.; Woodman, T.; Lloyd, M. A study on the chiral inversion of mandelic acid in humans. *Org. Biomol. Chem*. **2014**, *12*, 6737-6744.
38. Poláková, M.; Krajčovičová, Z.; Meluš, V.; Štefkovičová, M.; Šulcová**, M.** Study of urinary concentrations of mandelic acid in employees exposed to styrene. *Cent. Eur. J. Publ. Health* **2012**, *20*, 226-232.
39. McDougall, I. Thyroid cancer in clinical practice, Springer-Verlag London Limited 2007, 1-163.
40. Ivanova, B. Structural analysis of polylactic acid in composite starch biopolymers - a stochastic dynamics mass spectrometric approach. *Innov. Discov***. 2024**, *1*, 1-22.
41. Ivanova, B. Stochastic dynamics mass spectrometric and Fourier transform infrared spectroscopic structural analyses of composite biodegradable plastics. *Pollut. Study* **2024**, *5*, 2741.
42. Cheng, Y.; Jiao, Z.; Li, M.; Xia, M.; Zhou, Z.; Song, P.; Xu, Q.; Wei, **Z.** A new class of nucleating agents for poly(L-lactic acid): Environmentally-friendly metal salts with biomass-derived ligands and advanced nucleation ability. *Int. J. Biol. Macromol.* **2023**, *225*, 1599-1606.
43. Liao, H.; Feng, B.; Song, X.; Zhang, J.; Zhang, **Z.** Unlocking full potential of bamboo waster: Efficient co-production of xylooligosaccharides, lignin, and glucose through low-dosage mandelic acid hydrolysis with alkaline processing. *Int. J. Biol. Macromol*. **2024**, *282*, 137165.
44. Wang, S.; Liu, B.; Liang, J.; Wang, F.; Bao, Y.; Qin, C.; Liang, C.; Huang, C.; Yao, S. Rapid and mild fractionation of hemicellulose through recyclable mandelic acid pretreatment. *Biores. Technol*. **2023**, *383*, 129154.
45. Jeswani, H.; Perry, M.; Shaver, M.; Azapagic, A. Biodegradable and conventional plastic packaging: Comparison of life cycle environmental impacts of poly(mandelic acid) and polystyrene. *Sci. Tot. Environm*. **2023**, *903*, 166311
46. Wang, X.; China, A.; Tong, R. Controlled ring-opening polymerization of O-carboxyanhydrides to synthesize functionalized poly(α-hydroxy acids). *Org. Mater*. **2021**, *3*, 41-50.
47. Liu, T.; Simmons, T.; Bohnsack, D.; Mackay, M.; Smith, III, M.; Baker, G. Synthesis of polymandelide: A degradable polylactide derivative with polystyrene-like properties. *Macromol*. **2007**, *40*, 6040-6047.
48. Buchard, A.; Carbery, D.; Davidson, M.; Ivanova, P.; Jeffery, B.; Kociok-Kçhn, G.; Lowe, J. Preparation of stereoregular isotactic poly(mandelic acid) through organocatalytic ring-opening polymerization of a cyclic O-carboxyanhydride. *Angew. Chem. Int. Ed***. 2014**, *53*, 13858-13861.
49. Halder, P.; Chakraborty, B.; Banerjee, P.; Zangrando, E.; Paine, T. Role of α-hydroxycarboxylic acids in the construction of supramolecular assemblies of nickel(ii) complexes with nitrogen donor coligands. *CrystEngComm* 2009, *11*, 2650-2659.
50. Álvarez-Vidaurre, A.; Castiñeiras,A.; Frontera, A.; García-Santos, I.; Gil, D.; González-Pérez, Niclós-Gutiérrez, J.; Torres-Iglesias, R. Weak interactions in cocrystals of isoniazid with glycolic and mandelic acids. *Crystals* **2021**, *11*, 328.
51. Mao, Z.; Xia, K.; Zhang, K.; Chen, H.; Li, M.; Abdukader, A.; Jin, W. Visible light-induced oxidative esterification of mandelic acid with alcohols: a new synthesis of α-ketoesters. *Green Chem.* **2024**, *26*, 6046-6050.
52. Ahsan, M.; Varma, H.; Mishra, M.; Mukherjee, A. Template-sssisted visible light-induced [2+2] photodimerization in a pseudopolymorphic binary Solid: Topotacbc transformation vs photoinduced crystal melting. *Cryst. Growth Des*. **2024**, *24*, 5193-5199.
53. Patent: UNIVERSITY COLLEGE LONDON - WO2020/43866, 2020, A1.
54. Van Haren, M.; Thomas, M.; Sartini, D.; Barlow, D.; Ramsden, D.; Emanuelli, M.; Klamt, F.; Martin, N.; Parsons, P. The kinetic analysis of the N-methylation of 4-phenylpyridine by nicotinamide N-methyltransferase: Evidence for a novel mechanism of substrate inhibition. *Int. J. Biochem. Cell Biol*. **2018**, *98*, 127-136.
55. Maris, M.; Ferri, D.; Königsmann, L.; Mallat, T.; Baiker, A. Why are α-hydroxycarboxylic acids poor chiral modifiers for Pt in the hydrogenation of ketones? *J. Catal*. **2006**, *237*, 230-236.
56. Fu, Y.; Liu, X.; Zhao, S. Mandelic acid as an interfacial modifier for high performance NiO_x-based inverted perovskite solar cells. *ChemNanoMat* **2022**, *8*, e202200091.
57. Ivanova, B.; Spiteller, M. Matrixes in UV-MALDI mass spectrometry – crystals of organic saltsversus co-crystals of neutral polyfunctional carboxylic acids. *Anal. Methods* **2012**, *4*, 2247-2253.

 doi:10.20944/preprints202501.0504.v1

58. Marciniak, J.; Andrzejewski, M.; Cai, W.; Katrusiak, A. Wallach's rule enforced by pressure in mandelic acid. *J. Phys. Chem. C* **2014**, *118*, 4309-4313.
59. Cai, W.; Marciniak, J.; Andrzejewski, M.; Katrusiak, A. Pressure effect on D,L-mandelic acid racemate crystallization. *J. Phys. Chem. C* **2013**, *117*, 7279-7285.
60. Rose, H. Crystallographic Data. 61. dl-mandelic acid. *Anal. Chem.* **1952**, *24*, 1680-1681.
61. Wei, K.; Ward, D. α-Hydroxyphenylacetic acid: A redetermination. *Acta Cryst.* B, **1977**, *33*, 797-800.
62. Mughal, R.; Gillon, A.; Davey, R. DL-mandelic acid: CCDC 602882, 2006.
63. Fischer, A.; Profir, V. A metastable modification of (RS)-mandelic acid. *Acta Cryst. E* **2003**, *59*, 1113-1116.
64. Rietveld, I.; Barrio, M.; Tamarit, J.; Do, B.; Ceolin, R. Enantiomer resolution by pressure increase: Inferences from experimental and topological results for the binary enantiomer system (R)- and (S)-mandelic acid. *J. Phys. Chem.* B **2011**, *115*, 14698-14703.
65. Ellison, R.; Johnson, C.; Levy, H. Glycolic acid: direct neutron diffraction determination of crystal structure and thermal motion analysis. *Acta Cryst*. **1971**, *B27*, 333-344.
66. Bond, A.; Boese, R.; Desiraju, G. What is a polymorph? Aspirin as a case study. *Am. Pharmaceut. Rev*. **2007**, *2007*, 1-4.
67. Bond, A.; Solanko, K.; Parsons, S.; Redder, S.; Boese, R. Single crystals of aspirin form II: crystallisation and stability. *CrystEngComm* **2011**, *13*, 399-401.
68. Higashi, K.; Ueda, K. & Moribe, K. Recent progress of structural study of polymorphic pharmaceutical drugs. *Adv. Drug Del. Rev.* **2017**, *117*, 71-85.
69. Guo, S.; Zhu, W.; Zhang, C. Intralayer molecular packing coefficient as one packing characteristic of planar layer-stacked crystals and its dominators. *Cryst. Growth Des.* **2024**, *24*, 9849-9856.
70. Vasconcelos, S.; Tenorio, J.; Gurgel, J.; Benevides, C.; Nazario, C.; Carvalho Jr, P. Polymorphism of racemic (±)-Mefloquine free base: The role of enantiomeric recognition in polymorph assemblies. *J. Mol. Struct*. **2025**, *1325*, 141043.
71. Rietveld, I.; Barrio, M.; Tamarit, J.; Do, B.; Ceolin, R. Enantiomer resolution by pressure increase: Inferences from experimental and topological results for the binary enantiomer system (R)- and (S)-mandelic acid. *J. Phys. Chem. B* **2011**, *115*, 14698–14703.
72. Hylton, R.; Tizzard, G.; Threlfall, T.; Ellis, A.; Coles, S.; Seaton, C.; Schulze, E.; Lorenz, H.; Seidel-Morgenstern, A.; Stein, M.; Price, S. Are the crystal structures of enantiopure and racemic mandelic acids determined by kinetics or thermodynamics? *J. Am. Chem. Soc.* **2015**, *137*, 11095-11104.
73. Ivanova, B. Special Issue with Research Topics on "Recent Analysis and Applications of Mass Spectra on Biochemistry", *Int. J. Mol. Sci.* **2024**, *25*, 1995.
74. Nervall, M.; Hanspers, P.; Carlsson, J.; Boukharta, L.; Aqvist, J. Predicting binding modes from free energy calculations *J. Med. Chem.* **2008**, *51*, 2657-2667.
75. Cheng, Y.; Prusoff, W. Relationship between the inhibition constant (KI) and the concentration of inhibitor which causes 50 per cent inhibition (I_{50}) of an enzymatic reaction. *Biochem. Pharmacol*. **1973**, *22*, 3099-3108.
76. Wang, Y.; Su, Z.; Hsieh, C.; Chen, C. Predictions of binding for dopamine D_2 receptor antagonists by the SIE method. *J. Chem. Inf. Moled.* **2009**, *49*, 2369-2375.
77. Stewart, R.; Craven, R. Molecular electrostatic potentials from crystal diffraction: The neurotransmitter γ-aminobutyric acid. *Biophys. J*. **1993**, *65*, 998-1005.
78. Hirshfeld, F. Difference densities by least-squares refinement: fumaric acid. *Acta Cryst*. **1971**, *B27*, 769-781.
79. Stewart, R. On the mapping of electrostatic properties from Bragg diffraction data. *Chem. Phys. Lett.* **1979**, *65*, 335-342.
80. Stewart, R. Mapping electrostatic potentials from diffraction data. *God. Jugosl. Cent. Kristalogr*. **1982**, *17*, 1-24.
81. Spackman, M.; McKinnon, J. Jayatilaka, D. Electrostatic potentials mapped on Hirshfeld surfaces provide direct insight into intermolecular interactions in crystals. *CrystEngComm* **2008**, *10*, 377–388.
82. Spackman, M. Jayatilaka, D. Hirshfeld surface analysis. *CrystEngComm* **2009**, *11*, 19-32.
83. Bader, R. Atoms in Molecules - A Quantum Theory, Oxford University Press, Oxford, 1990.
84. Suda, S.; Tateno, A.; Nakane, D.; Akitsu, T. Hirshfeld surface analysis for investigation of intermolecular interaction of molecular crystals. *Int. J. Org. Chem*. **2023**, *13*, 57-85.

85. Datt, I.; Ozerov, P. Presicion study of the electron density distributed in molecules and crystals from diffraction data. *Zhurnal Strukt. Khim*. **1975**. *16*, 509-535.
86. Van Damme, S.; Bultinck, P.; Fias, S. Electrostatic potentials from self-consistent Hirshfeld atomic charges. *J. Chem. Theory Comput*. **2009**, *5*, 334–340.
87. Hirshfeld, F. Bonded-atom fragments for describing molecular charge densities. *Theoret. Chim. Acta (Berl.)* **1977**, *44*, 129-138.
88. Hirshfeld, F. Shmueli, U. Covariances of thermal parameters and their effect on rigid-body calculations. *Acta Cryst*. **1972,** *A28*, 648-652.
89. Kuriyan, J.; Petsko, G.; Levy, R.; Karplus, M. Effect of anisotropy and anharmonicity on protein crystallographic refinement. An evaluation by molecular dynamics. *J. Mol. Biol*. **1986**, *190*, 227-254.
90. Cruickshank, D. The variation of vibration amplitudes with temperature in some molecular crystals. *Acta Cryst*. **1956**, *9*, 1005-1009.
91. Ivanova, B.; Spiteller, M. Ag^{I} and Zn^{II} complexes with possible application as NLO materials – Crystal structures and properties. *Polyhedron* **2011**, *30*, 241-245.
92. Coppens, P.; Csonka, L.; Willoughby, T. Electron population parameters from least-squares refinement of X-ray diffraction data. *Science* **1970**, *167*, 1126-1128.
93. Mangaiyarkkarasi, M.; Saravanan, R.; Ismail, M. Chemical bonding and charge density distribution analysis of undoped and lanthanum doped barium titanate ceramics. *J. Chem. Sci*. **2016**, *128*, 1913-1921.
94. Aubert, E.; Lebegue, S.; Marsman, M.; Bui, T.; Jelsch, C.; Dahaoui, S.; Espinosa, E.; Angyan, J. Periodic projector augmented wave density functional calculations on the hexachlorobenzene crystal and comparison with the experimental multipolar charge density model. *J. Phys. Chem.* A **2011**, *115*, 14484-14494.
95. Hirano, Y.; Takeda, K.; Miki, K. Charge-density analysis of an iron–sulfur protein at an ultra-high resolution of 0.48 Å. *Nature* **2016**, *534*, 281-284.
96. Thomas, S.; Pavan, M.; Row, T.; Experimental evidence for 'carbon bonding' in the solid state from charge density analysis. *Chem. Commun*. **2014**, *50*, 49-51.
97. Weinhold, F.; Landis, C. Discovering Chemistry with Natural Bond Orbitals, Wiley, Hoboken, NJ, 2012, 1-319.
98. Brown, I. The chemical bond in inorganic chemistry, The bond valence model, Oxford science publications, 2002, Oxford.
99. Brown, I. Recent developments in the methods and applications of the bond valence model. *Chem. Rev*. **2009**, *109*, 6858-6919.
100. [http://shelx.uni-ac.gwdg.de/SHELX/bv-method.pdf; http://shelx.uni-ac.gwdg.de/SHELX/complex_eden.pdf].
101. Escudero, E.; Bauz, A.; Frontera, A.; Ballester, P. Nature of noncovalent carbon-bonding interactions derived from experimental charge-density analysis. *ChemPhysChem* **2015**, *16*, 2530-2533.
102. Blanksby, S.; Ellison, G. Bond dissociation energies of organic molecules. *Accts. Chem. Res*. **2003**, *36*, 255-263.
103. Stalke, D. (Ed.), Electron density and chemical bonding I, Springer's series 'Structure and Bonding', Springer Verlag, berlin Heidelberg, 2012, 1-212.
104. Ivanova, B.; Spiteller, M. On the nature of the coordination bonding of metal–organics for ions with the d10 electronic configuration – Experimental and theoretical analyses. *Polyhedron* **2017**, *137*, 256-264.
105. Abramov, Y. On the possibility of kinetic energy density evaluation from the experimental electron-density distribution *Acta. Cryst*. **1997**, *A53*, 264-272.
106. Ivanova, B.; Spiteller, M. Crystallographic and theoretical study of the atypical distorted octahedral geometry of the metal chromophore of zinc(II) bis((1R,2R)-1,2-diaminocyclohexane) dinitrate. *J. Mol. Struct*. **2022**, *1248*, 131488.
107. Marenich, A.; Jerome, S.; Cramer, C.; Truhlar, D. Charge Model 5: An extension of Hirshfeld population analysis for the accurate description of molecular interactions in gaseous and condensed phases. *J. Chem. Theor. Comput.* **2012**, *8*, 527-541.

 doi:10.20944/preprints202501.0504.v1

108. Badawi, H.; Förner, W.; Ali, S. A study of the solvent dependence of the structures and the vibrational, ^{1}H and ^{13}C NMR spectra of L- and DL-mandelic acid and L- and DL-3-phenyllactic acid. *J. Mol. Struct*. **2015**, *1093*, 150-161.
109. Da Silva, C.; Guimarães, F.; Ribeiro, L.; Martins, F. Salt or cocrystal of salt? Probing the nature of multicomponent crystal forms with infrared spectroscopy. *Spectrochim. Acta* **2016**, *167A*, 89-95.
110. Wang, Z.; Duan, S.; Zhang, R.; Ma, L.; Lin, K. Rapid chiral purity identification of mandelic acid by Raman spectra in the O–H stretching region. *Spectrochim. Acta* **2023**, *303A*, 123251.
111. Barth, G.; Voelter, W.; Mosher, H.; Bunnenberg, E.; Djerassi, C. Optical rotatory dispersion studies. CXVII.1 Absolute configurational assignments of some α-substituted phenylacetic acids by circular dichroism measurements. *J. Am. Chem. Soc.* **1970**, *92*, 875-886.
112. Ivanova, B.; Spiteller, M. Stochastic dynamic electrospray ionization mass spectrometric diffusion parameters and 3D structural determination of complexes of Ag^{I}-ion – Experimental and theoretical treatment. *J. Mol. Liq*. **2019**, *292*, 111307.
113. Blessing, R. An empirical correction for absorption anisotropy. *Acta Crystal*. **1995**, *A51*, 33-38.
114. Sheldrick, G. A short history of SHELX. *Acta Crystal.* **2008**, *A64*, 112-122.
115. Sheldrick, G. Experimental phasing with SHELXC/D/E: combining chain tracing with density modification. *Acta Crystal*. **2010**, *D66*, 479-485.
116. Sheldrick, G. Phase annealing in SHELX-90: direct methods for larger structures. *Acta Crystal*. **1990,** *A46*, 467-473.
117. Spek, A. Single-crystal structure validation with the program PLATON. *J. Appl. Cryst*. **2003**, *36*, 7-13.
118. [http://www.ccp14.ac.uk/ccp/web-mirrors/mallinson/~paul/xd.html].
119. Momma, K.; Ikeda, T.; Belik, A.; Izumi, F. Dysnomia, a computer program for maximum-entropy method (MEM) analysis and its performance in the MEM-based pattern fitting. *Powder Diffr*. **2013**, *28*, 184-193.
120. Le Page, Y. Computer derivation of the symmetry elements implied in a structure description. *J. Appl. Cryst.* **1987**, *20*, 264-269.
121. Le Page, Y. MISSYM 1.1 - a flexible new release. *J. Appl. Cryst.* **1988**, *21*, 983-984.
122. Spek, A. CheckCIF validation ALERTS: what they mean and how to respond. *Acta Cryst*. **2020**, *76*, 1-11.
123. Linden, A. Obtaining the best results: aspects of data collection, model finalization and interpretation of results in small-molecule crystal-structure determination. *Acta Cryst*. **2020**, *E76*, 765-775.
124. [http://www.crystallography.fr/crm2/fr/services/logiciels/MoPro.htm]
125. [http://www.chem.gla.ac.uk/~louis/software/wingx/].
126. Dunitz, J.; Schomaker, V.; Trueblood, K. Interpretation of atomic displacement parameters from diffraction studies of crystals. *J. Phys. Chem.* **1988**, *92*, 856-867.
127. Dunitz, J.; Maverick, E.; Trueblood, K. Atomic motions in molecular crystals from diffraction measurements. *Angew. Chem., Int Ed*. **1988**, *27*, 880-895.
128. Huebschle, C.; Sheldrick, G.; Dittrich, D. ShelXle: a Qt graphical user interface for SHELXL. *J. Appl. Crystallogr*. **2011**, *44*, 1281-1284.
129. Ivanova, B. (2025). Supporting information data. Zenodo. [https://doi.org/10.5281/zenodo.14601517] (available at 05.01.2025).
130. Frisch, M.; Trucks, G.; Schlegel, H.; Scuseria, G.; Robb, M.; Cheeseman, J.; Fox, D. (1998, 2009), Gaussian 09, 98, Gaussian, Inc., Pittsburgh, Wallingford CT.[www.gaussian.com].
131. Helgaker, T.; Jensen, H.; Jrgensen, P. et al. Dalton Program Package; 2011; [http://www.daltonprogram.org/download.html].
132. Gordon, M.; Schmidt, M. Advances in electronic structure theory: GAMESS a decade later, in "Theory and Applications of Computational Chemistry: the first forty years" C. Dykstra, G. Frenking, K. Kim, G. Scuseria (Eds.,) Elsevier, Amsterdam, 2005; 1167-1189.
133. Nielsen, A.; Holder, A. Gauss View 5.0, User's Reference. GAUSSIAN Inc., Pittsburgh GausView03 Program Package, 2009; [*www.gaussian.com/g_prod/gv5.htm].*
134. Burkert, U.; Allinger, N. Molecular mechanics in ACS Monograph 177, American Chemical Society, Washington D.C. 1982; pp. 1-339.

 doi:10.20944/preprints202501.0504.v1

135. Allinger, L. Conformational analysis. 130. MM2. A hydrocarbon force field utilizing V1 and V2 torsional terms. *J. Am. Chem. Soc*. **1977**, *99*, 8127-8134.
136. Macetti, G.; Genoni, A. Quantum mechanics/extremely localized molecular orbital modelling strategy for excited states: Coupling to time-dependent density functional theory and equation-of-motion coupled cluster. *J. Chem. Theory Comput*. **2020**, *16*, 7490-7506.
137. Stanton, J.; Bartlett, R. The equation of motion coupled cluster method. A systematic biorthogonal approach to molecular excitation energies, transition probabilities, and excited state properties. *J. Chem. Phys*. **1993**, *98*, 7029-7039.
138. Krylov, A. Equation-of-motion coupled-cluster methods for open-shell and electronically excited species: The hitchhiker's guide to Fock space. *Annu. Rev. Phys. Chem*. **2008**, *59*, 433.
139. Reshetova, E. Effect of the ionic strength of a mobile phase on the chromatographic retention and thermodynamic characteristics of the adsorption of enantiomers of phenylcarboxylic acids on a chiral adsorbent with grafted antibiotic eremomycin. *Russian J. Phys. Chem. A* **2017**, *91*, 167-174.
140. OpenOffice [http://de.openoffice.org].